Rainbow Cherenkov Second-Harmonic Radiation

Lihong Hong,[1] Baoqin Chen,[1] Chenyang Hu,[2] Peng He,[2] and Zhi-Yuan Li[1,*]

[1] *School of Physics and Optoelectronics, South China University of Technology, Guangzhou 510641, China*
[2] *Guangdong Jingqi Laser Technology Corporation Limited, Songshanhu, Dongguan 523808, China*

(Received 19 March 2022; accepted 26 September 2022; published 26 October 2022)

Nonlinear Cherenkov radiation, an intriguing noncollinear optical parametric process with versatile longitudinal phase matching, is commonly realized in engineered nonlinear photonic structures. Here, we report on the observation of ultrabroadband rainbow Cherenkov second-harmonic generation (UBR CSHG) in a single periodically poled lithium niobate (PPLN) nonlinear crystal driven by a near-infrared high-peak-power ultrashort femtosecond pump laser. Multiple colored nonlinear radiation bands along the direction of Cherenkov conical angles are simultaneously exhibited, leading to a beautifully colorful rainbow picture never reported before. We systematically analyze the multicolor spectral characteristics of the UBR CSHG in the whole conical direction and explicitly clarify their phase-matching conditions. We show that this UBR CSHG interaction is subject to remarkable spectral broadening owing to both the third-order nonlinearity effect induced by the high-peak-power ultrashort pump laser and the reciprocal lattice vector of the PPLN crystal, which eventually enables the generation of three bright dominating colors—red, orange-yellow, and green bands—and their automatic dispersion in space. The experimental results suggest rich physics of nonlinear optical interactions and indicate the possibility to engineer broadband nonlinear frequency conversion for applications in compact colored laser sources and others.

DOI: 10.1103/PhysRevApplied.18.044063

I. INTRODUCTION

Second-harmonic generation (SHG), one of the most extensively investigated nonlinear parametric processes of a laser interacting with nonlinear crystals, is usually implemented under two popular phase-matching schemes: the birefringent phase-matching technique [1] and the quasi-phase-matching (QPM) technique [2]. Generally, QPM technology is used for collinear propagation between the interacting waves along the QPM-grating wave vector, in periodic [3], quasiperiodic [4], and periodic nonlinear optical lattices [5–7], as well as superlattices [8]. In addition to QPM, several noncollinear SHG processes have attracted extensive and intensive interest [9–11]; one of them is the Cherenkov second-harmonic generation (CSHG) [12]. This phenomenon is an optical close analog of the famous Cherenkov effect, where a charged particle moving faster than the speed of the light in media then emits conical Cherenkov radiation [13]. Similarly, in such a nonlinear optical process, the second-harmonic wave (SHW) appears in the form of a conical wave with respect to the transmission direction of the pump's fundamental wave (FW).

Theoretical and experimental investigations into such CSHG processes are widely reported in bulk nonlinear optical crystal [12,14–21] or waveguide geometries [22–28]. These publications all reveal that the CSHG can efficiently occur just by requiring the fulfillment of longitudinal phase-matching conditions, which vastly relaxes the stringent phase-matched requirements. Besides, these interesting CSHG processes have some practical applications, such as nonconventional characterization and measurement for planar waveguides [29,30], the characterization and single-shot reconstruction of femtosecond pulses [31,32], and optical imaging of ferroelectric domain walls [33,34].

Nowadays, Cherenkov radiation, whether in optical waveguides or in bulk crystals, is usually realized upon illumination of a monochromatic pump light [22] or a short-pulse laser with a very narrow bandwidth [16,17,21] via the second-order nonlinearity (2NL) of the domain walls or the polarization discontinuity between the waveguide and the substrate. Nonetheless, the Cherenkov scheme obtained only by second-order nonlinear effects has certain limitations in performance. First, the severe limitation is the nonlinear working bandwidth, namely, the spectral bandwidth where sufficiently efficient conversion from the pump to emitted-signal laser via the nonlinear crystal is quite narrow, usually at the level of several

*phzyli@scut.edu.cn

nanometers. Furthermore, there are no abundant different frequency components of the Cherenkov output signals to support continuous spatial separation, a phenomenon like the "rainbow," popular in nature. As a consequence, the radiation patterns obtained are always single-color or quite narrowband rings. In our previous work, we demonstrated that a mid-infrared femtosecond pulse laser could facilitate the production of an ultrabroadband visible white-light beam in the collinear QPM mechanism [6]. Furthermore, we observed that a high-peak-power femtosecond laser could ignite a significant third-order nonlinearity (3NL) effect to supplement the 2NL effect for creating the visible to near-infrared supercontinuum white laser [35]. It is natural to pose the question of whether the high-peak-power ultrashort femtosecond pump laser might bring about something new in the noncollinear CSHG processes, and whether the 3NL also has a significant influence on Cherenkov radiation.

Here, we present noticeable experimental demonstrations of an ultrabroadband rainbow (UBR) CSHG in a single periodically poled lithium niobate (PPLN) nonlinear crystal pumped by a near-infrared high-peak-power ultrashort femtosecond laser pulse. We systematically investigate the spectral properties of the rainbow Cherenkov emissions and their radiation performance in different conical angles. The greatly enhanced spatial dispersion and expansion feature of the radiation arcs along the $\chi^{(2)}$ modulation direction is characterized using the phase-matched QPM CSHG concept. Subsequently, we show how the rainbow capacity of CSHG can be further enhanced based on the modulation of the pump-laser power as well as the usage of the QPM mechanism.

II. NONLINEAR OPTICAL EXPERIMENTS

In our experiment, the sample used is a z-cut PPLN with a period of 6.96 μm and a duty ratio of 1:1. Here, we fabricate the PPLN samples by using the electric poling technique at room temperature. Standard optical-grade z-cut LN crystals of 1 mm thick are used as the raw material. The dimensions of the PPLN sample are 5 (x) × 20 (y) × 1 mm^3 (z). For a typical PPLN sample, the microscopic details of positive and negative poled domains are explicitly illustrated in Figs. 1(a) and 1(b), and the fabricated PPLN sample is schematically displayed in Fig. 1(c). A schematic experiment diagram is illustrated in Fig. 1(d). Here, for clarity of viewing and discussion, the coordinate system is set so that the incident laser beam propagates along the $+z$-axis direction, the PPLN sample has its surface normal parallel to the z axis, and its poling domains walls extend along the x-axis direction and are modulated along the y-axis direction. The input pump beam is a near-infrared femtosecond laser at a central wavelength of 1300 nm, pulse duration of 50 fs, repetition rate of 1 kHz, average power of 20–70 mW, and energy per pulse of 20–70 μJ. The input femtosecond pulse laser has a rich bandwidth of about 100 nm. The fundamental beam, which is linearly x polarized, namely, parallel to the PPLN domain walls, is directed at normal incidence, illuminated upon the x-o-y surface of the PPLN sample, and propagates along the z axis. Then two types of SHG processes are possible: two ordinary waves act to generate an ordinary SHW, namely, [oo-o], and two ordinary waves act to generate an extraordinary SHW, namely, [oo-e]. The utilized elements in the $\chi^{(2)}$ tensor of these parametric processes correspond to d_{11} and d_{11}, together with d_{31}, respectively [16,17,36,37]. Here, the beam is loosely focused into the sample with a $1/e^2$ spot diameter size of about 1 mm. A long-pass filter is placed in front of the PPLN crystal sample, which is used to filter some mixed signals of visible-light output from the optical parametric amplifier (OPA) and only passes wavelengths above 950 nm to ensure the correctness of the CSHG experimental results. Then, the CSHG signal emitted from the crystal is projected onto a screen located 4.45 cm behind the sample and recorded with a Nikon D7200 camera. For such a given input power, the peak intensity of the pump FW laser corresponds to 51–178 GW/cm^2, and it is well below the optical damage threshold for our PPLN sample of about 200 GW/cm^2. It is easy to induce remarkable 3NL processes, such as self-phase modulation, by such a high level of laser intensity. Here, we observe spectral broadening when the pump femtosecond laser transmits along the optical axis of the z-cut PPLN crystal. The pump power is first set to 60 mW, and the corresponding spectrum is displayed in Fig. 1(e). The bandwidth of the input femtosecond pulse laser is slightly below 100 nm, while that of the output femtosecond pulse laser is greatly expanded up to a total value of about 200 nm, exhibiting 2 times spectral broadening. In analogy with the collinear QPM case [35], this powerful 3NL may work well with the noncollinear CSHG process and make the output signals have a much larger bandwidth.

III. RESULTS AND DISCUSSION

A. Rainbow Cherenkov radiation in PPLN

In Fig. 2(a), we show the overall Cherenkov radiation pattern recorded from the PPLN sample, where the distance between the screen and the end face of the crystal is 4.45 cm. As seen in Fig. 2(a), the radiation pattern projected on the screen consists of two parts. One is the Cherenkov second-harmonic structure that involves a beautifully colorful pattern like a rainbow, which is composed of colorful bands with red, orange-yellow, and green. Such an attractive phenomenon is the main body of this work. The other part, inside the rings, close to the center, is another phase-matching configuration named Raman-Nath diffraction, which is strongly dependent on the type of poled patterns [6,36] and will be explored

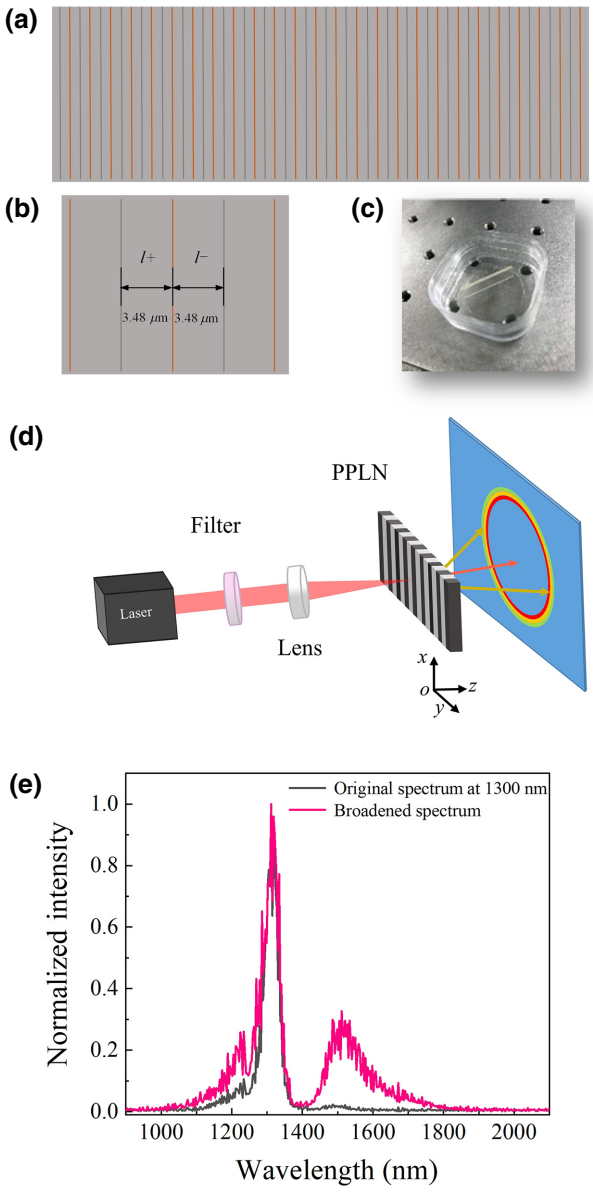

FIG. 1. Experiment layout. (a) Microscopic image of the fabricated sample surface of a typical one-dimensional (1D) PPLN structure. (b) High-magnification view of the PPLN sample. (c) Fabricated PPLN sample. (d) Experimental setup. (e) Spectral broadening for the pump-laser pulse with a central wavelength of 1300 nm passing through a PPLN crystal at an input power of 60 mW.

deeply in our future work. To better study the properties of this multicolor Cherenkov radiation in our experiment, we perform a comprehensive analysis of the circular arcs in different directions. First, we focus on the CSHG arcs distributed in the west and east directions of the screen, as depicted in Figs. 2(b) and 2(c). The arcs of these distinct colored bands are marked with *a–f* . The emitted bands are observed by eye to change color from red to yellow to green in both west and east directions. Meanwhile, we can observe that arcs *a–c* in the west are symmetric with respect to *d–f* in the east, respectively. To further prove the polychromatic property of this radiation, we place a 1-mm-wide slit monitor, which is just capable of covering a single-color band, behind the end face of the PPLN sample at a distance of about 1.4 cm, and move it perpendicular to the CSHG beam to measure the spectra at different transverse positions of the CSHG bands. As shown in Fig. 2(d), the spectra of the CSHG emissions in areas *a–f* are found to involve a series of rainbow bands covering approximately 593–832, 527–768, 493–713, 588–838, 555–746, and 513–745 nm, respectively. Note that the parts of UBR CSHG emission along the west and east directions exhibit three prominent color bands, 493–745, 527–768, and 593–838 nm, which correspond to three main color regions: green (492–577 nm), orange-yellow (577–622 nm), and red (622–780 nm). All these frequency components add up to form the smooth broadband CSHG spectrum, ranging approximately from 493 to 838 nm. We expect that this brilliant rainbow feature comes from the frequency doubling of the fundamental laser light at 1300 nm with a broadening bandwidth up to 200 nm due to the additional 3NL.

In addition, one can find several other unique features. For example, significant chromatic broadening exists in each of the three regions *a–c* (or *d–f*), where the spatial bandwidths show a trend of gradual increase, which is approximately 3, 6, and 8 mm, respectively. Especially, this feature of chromatic broadening is more obvious in the shorter-wavelength bands. We expect these arcs are modified Cherenkov radiation, which involves the action of reciprocal vectors through the so-called phase-matched QPM CSHG process. Compared with the direct Cherenkov configuration, the forward and backward reciprocal vectors, which correspond to the positive-order and negative-order reciprocal vectors of the PPLN sample, respectively, may all participate in this modified CSHG process. Here, the involvement of reciprocal lattice vectors (RLVs) of the 1D PPLN crystal may work to facilitate the expansion of radiation angles and the broadening of spectral ranges.

B. Principle of phase-matched UBR CSHG

The process of Cherenkov frequency doubling is characterized by the direction of SHW emission defined solely by the longitudinal phase-matching condition, as shown in Fig. 3(a), which is

$$k_2 \cos\,\theta - 2k_1 = 0, \tag{1}$$

where k_1 and k_2 are the wave vectors of the FW and SHW monochromatic light transport within the nonlinear medium, respectively. θ represents the internal angle of the CSHG, and the corresponding external angle is marked as β. Under such conditions, the emitted pattern is a single-color ring.

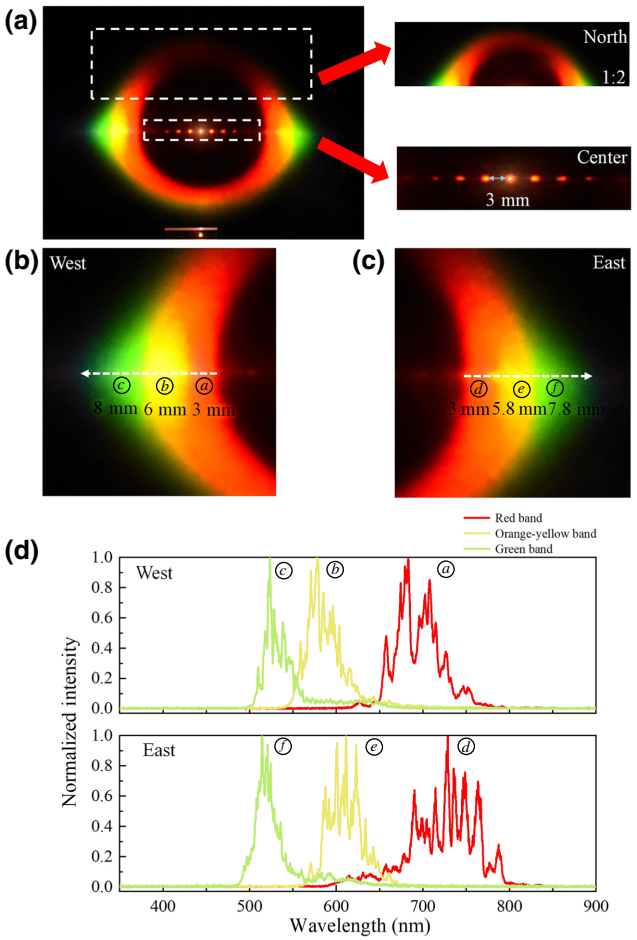

FIG. 2. Rainbow Cherenkov radiation generated in the PPLN sample with an incident femtosecond pump laser at 1300 nm with an input power of 60 mW. (a) Photographs of multicolor rainbow Cherenkov second-harmonic generation. Measured ratio between the overall radiation and the enlarged graphs on the right is about 1:2. (b),(c) Locally enlarged images of the Cherenkov arcs in the west and east directions, where the different colored areas are marked as *a*–*f* . (d) Ultrabroadband rainbow spectrum (normalized against the peak intensity) of the Cherenkov arcs in areas *a*–*f* .

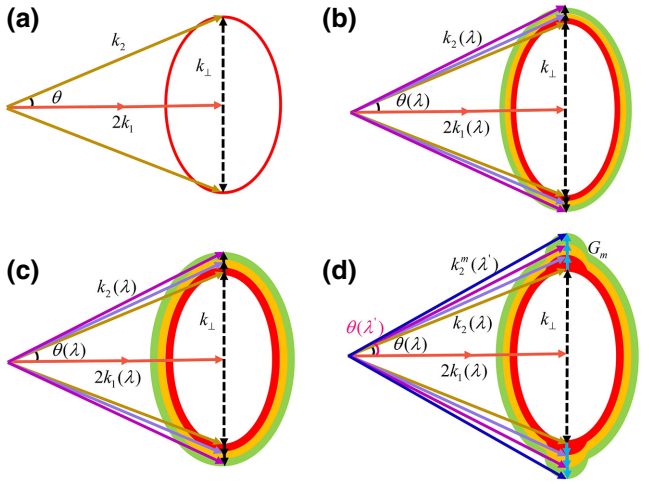

FIG. 3. Principle of phase matching for generating the UBR CSHG laser in the PPLN nonlinear crystal. (a) Phase-matching diagram for monochromatic CSHG in nonlinear crystals via the 2NL process for monochromatic pump light. (b) Phase-matching diagram for broadband rainbow CSHG via the 2NL process for the ultrashort pump-laser pulse. (c) Phase-matching diagram for UBR CSHG via synergic action of 2- and 3NL for the high-peak-power femtosecond pump laser. (d) Phase-matching diagram for broadening UBR CSHG via synergic action of 2- and 3NL combined with the effect of the RLVs.

When the incident light is an ultrashort laser pulse with a very large operation bandwidth, the involved phase-matching diagram of the CSHG should be described as a polychromatic mechanism, which is rewritten as

$$k_2(\lambda)\cos\,\theta(\lambda) - 2k_1(\lambda) = 0, \tag{2}$$

where $k_1(\lambda)$ and $k_2(\lambda)$ represent the wave vectors of each spectral component at λ for the FW and SHW ultrashort laser pulses in the nonlinear crystal, respectively. We can expect different frequency components of the CSHG signals to remain separated in space, i.e., different conical angle θ, benefiting from this longitudinal phase-matching condition. As clearly illustrated in Fig. 3(b), the recorded CSHG pattern possesses rainbowlike multiple-color bands due to the distinguished broad bandwidth of the ultrashort pump laser. Besides, as we point out, the 3NL enabled by the peak power of the pump laser will contribute to significant spectral broadening of the interacting waves, and new spectral components are added to the CSHG process as the pump-laser pulse proceeds through the crystal. Consequently, the synergic action of these 2NL and 3NL effects can result in an ultrabroadband rainbow CSHG pattern and produce a more significantly broadened spectrum, as depicted in Fig. 3(c).

A notable feature of UBR CSHG shown in Figs. 2(b) and 2(c) is the existence of bright broadening arcs along the $\chi^{(2)}$ modulation direction. A comprehensive interpretation for the occurrence of this feature could be given by introducing the QPM Cherenkov configuration for the 1D nonlinear photonic crystal. In this configuration, phase matching is automatically achieved by the effect of RLVs within the PPLN crystal. Here, we adequately explore the principle of this modified type of so-called QPM CSHG. The geometry of the QPM CSHG is summarized in Fig. 3(d), which exhibits that Cherenkov arcs occurring in the direction of the poled domain structure can have more broadened polychromatic bands with the participation of multiple RLVs. The general vectorial phase-matching conditions can be expressed in the following

TABLE I. Experimental and theoretical external emission angles of UBR CSHG in three dominating color bands. β_T and β_E represent theoretical and experimental Cherenkov external angles, respectively, for the red, orange-yellow, and green bands.

Red band		Orange-yellow band		Green band	
β_T (622–900 nm)	β_E	β_T (577–622 nm)	β_E	β_T (525–577 nm)	β_E
$24.7^\circ - 32.3^\circ$	$26.3^\circ - 29.3^\circ$	$32.3^\circ - 35.1^\circ$	$29.3^\circ - 34.9^\circ$	$35.1^\circ - 39.5^\circ$	$34.9^\circ - 41.2^\circ$
$\Delta = 7.6^\circ$	$\Delta = 3.0^\circ$	$\Delta = 2.8^\circ$	$\Delta = 5.6^\circ$	$\Delta = 4.4^\circ$	$\Delta = 6.3^\circ$

form:

$$\begin{aligned} &k_2(\lambda)\cos\ \theta(\lambda) - 2k_1(\lambda) = 0, \\ &k_2(\lambda)\sin\ \theta(\lambda) + G_m = k_2^m(\lambda')\sin\ \theta(\lambda'), \\ &\quad m = 0, \pm 1, \pm 2, \ldots . \end{aligned} \tag{3}$$

Here, $k_1(\lambda)$ and $k_2^m(\lambda')$ are the wave vectors of the FW and SHW ultrashort laser beams in this QPM CSHG process. $k_2(\lambda)$ represents the original wave vector of the SHW signal in the case of no RLVs. G_m is the mth-order RLV of the $\chi^{(2)}$ modulation, $G_m = m(2\pi/\Lambda)(\Lambda = 6.96\ \mu\text{m})$. $k_\perp$ is the phase mismatch. The RLV G_m is relative to the direction of $k_\perp$ [along the y-axis direction in Fig. 1(d)]. Here, this hybrid process is more complicated but more general. With $G_m = 0$, Eq. (3) returns to conventional Cherenkov radiation, as described by Eq. (2). On the basis of the law of refraction, the external conical angle outside the PPLN crystal is denoted by β, which is in the form of

$$\sin\beta_{o/e} = n_{2,o/e}(\lambda', \theta)\sin[\cos^{-1}(2k_{1,o}(\lambda)/k_{2,o/e}^m(\lambda'))], \tag{4}$$

where $n_{2,o/e}(\lambda', \theta)$ is the index of refraction of the Cherenkov harmonic radiation of ordinary or extraordinary waves. Looking closely into Eqs. (3) and (4), it is easy to see that this modified phase-matched QPM CSHG can be extended in both the emitted angles and the overall chroma with the participation of the forward and backward RLVs compared with the direct CSHG case. As an example, for a fundamental beam of 1300 nm, we can calculate that, with the effect of the first-order forward reciprocal vector, G_{+1}, the expanded offset of the spatial angle is about 6°, which corresponds to the lateral translation of about 7 mm in space. The bands near the center of the CSHG ring are associated with the backward G_m, and the bands away from the center involve the forward G_m. Table I gives the experimental and theoretical Cherenkov external angles for the red, orange-yellow, and green bands, where the theoretical bands are divided according to the pump spectrum, as shown in Fig. 1(e). The theoretical results are calculated under the conditions without participation from the RLVs. The exit angle ranges of the red, orange-yellow, and green bands in this experiment are measured to be about $26.3^\circ - 29.3^\circ$, $29.3^\circ - 34.9^\circ$, and $34.9^\circ - 41.2^\circ$, respectively, which are rather different from the values of the direct CSHG cases. These results hint at the possibility of QPM CSHG in the frequency-conversion process with both the compensation of backward and forward RLVs. It can be calculated that the RLVs of the first four orders ($m = \pm 1, \pm 2$) participate in the Cherenkov radiation in this experiment. Moreover, in the visible bands, CSHG radiation signals are more enlarged in the shorter-wavelength parts along the direction of the poled domain with greatly expanded radiation angles. From Fig. 2(b), we find that the bandwidths of the three colored bands along the $\chi^{(2)}$ modulation direction correspond to about 3, 6, and 8 mm, respectively. All experimental results are very consistent with our theoretical analysis of the principle of phase-matched UBR CSHG.

C. Radiation performance of the whole conical angles

By adjusting the angular position of the slit monitor precisely, we can obtain the spectral distributions of the CSHG frequency components in other distinct conical angles. The results are shown in Fig. 4. Here, we focus on some representative patterns of Cherenkov rings at the opposite angles of 0° and 180°, 60° and 240°, and 120° and 300°, with the vertical central line along the clockwise direction. It can be seen intuitively from Fig. 4(a) (and the enlarged pictures in Fig. 2) that the circular patterns of the six areas 1–6 are bright in the red band, while the yellow band and green band are relatively fainter. To see more details, we further measure the spectral curves of these emitted bands in these arc directions. The spectral envelope of the CSHG emissions in areas 1–6 are found to involve a series of rainbow bands covering approximately 533–717, 529–722, 525–734, 500–734, 500–766, and 515–737 nm, respectively. In short, the spectra of the output CSHG laser cover a series of red, orange-yellow, and green bands ranging approximately from 500 to 766 nm in these conical angles. Comparing these cases with Figs. 2(b) and 2(c), it can be found clearly that the rainbow features gradually broaden as the azimuth angles of the Cherenkov arcs get closer to the RLV directions; as such, the Cherenkov arcs in the west and east directions show relatively more prominent rainbow characteristics than in other orientations. The greatly expanded rainbow features approximately appear in the zones of ±5° away from the east-west directions. Beyond these areas, the overall performance in the radiation angle, light chroma, and spectral range of CSHG arcs is slightly weakening, but they still exhibit apparent multicolored-band features.

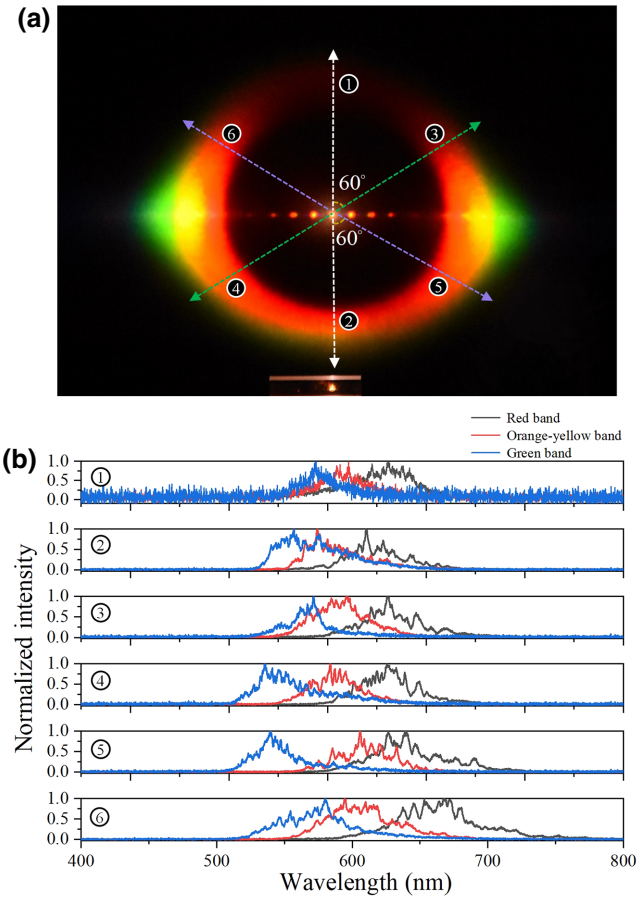

FIG. 4. Cherenkov performance in different azimuthal angles. (a) Pattern of Cherenkov rings at every two opposite angles of 0° and 180°, 60° and 240°, and 120° and 300°, with the vertical central line along the clockwise direction, which are marked as areas 1–6, respectively. (b) Normalized supercontinuum spectra of Cherenkov bands emitted from the designed PPLN sample at these fixed directions.

It should be pointed out that the rainbow performance of the UBR CSHG not only covers the RLV modulation directions but also covers the tunable range of the whole emitted angles.

Here, we would like to stress two important features of the generated pattern in our experiment. (i) The existence of conical rings rather than a pair of symmetrical spots in a 1D PPLN sample. The major reason is that the periodical structure in PPLN can provide more domain walls that can be covered by the FW beam; hence, the nonlinear polarizations driven by fundamental beams can be treated as isotropic and superpose with the wave vectors lying on a cone, resulting in the formation of a circular CSHG beam. (ii) A marked directionality of the CSHG patterns. It is shown that polarization of the input beam determines the azimuthal-intensity modulation of the CSHG pattern [16,17,36,37]. The CSHG pattern in our experiment is obtained with only one perpendicular symmetry plane and exhibits a darker upper semicircle [as displayed in Fig. 2(a)] when the PPLN is illuminated with a linearly x-polarized fundamental beam. This asymmetric phenomenon is mainly due to the following two reasons. First, the fundamental wave is a linearly x-polarized beam, so that there will be the coexistence of two types of SHG processes, [oo-e] and [oo-o], due to the birefringence of LN. Furthermore, there is a marked azimuthal dependence of the SHG intensity, which, in turn, depends on the type of SHG process. More precisely, the azimuthal modulation of the Cherenkov SH rings in LN features one maximum in the south for the extraordinary wave, and two maxima in the west and east and two minima in the north and south for the ordinary wave. As a consequence of these two factors, the colorful rainbow CSHG pattern becomes darker in the north, brighter in the south, and of course brightest in the east and west. On the other hand, it is feasible to manipulate the nonlinear optical response for this UBR CSHG process by tailoring the polarization state of the pump laser.

D. Rainbow variation dependent on the pump-laser power

Furthermore, we explore the dependence of the rainbow capability of CSHG on the input pump power. In the experiment, the incident FW power is increased from 20.1 to 70 mW with an interval of about 10 mW. The measured CSHG patterns are recorded by a camera and illustrated in Fig. 5. We compare the CSHG patterns produced by these six fundamental beams of different powers. The results observed in Fig. 5 show that the CSHG rings are sensitive to the increased power of the fundamental beams, which is easily detected by the naked eye to change from a single red band to ultrabroadband three-colored bands. Accordingly, the overall chroma of the output CSHG laser varies with the pump power. Looking closely at Figs. 5(a) and 5(b), we find that, when the pump laser is at lower powers of 20.1 and 30 mW, the observed CSHG has only a red band, and there is no obvious broadband rainbow feature at this time. As the input power increases to 40.1 mW, as displayed in Fig. 5(c), multicolor bands along the $\chi^{(2)}$ modulation direction (i.e., the east and west directions) begin to emerge, involving orange-yellow and green bands, but CSHG arcs in other directions are still just red bands. Continuing to increase the pump power to 50 mW, as illustrated in Fig. 5(d), the overall CSHG pattern in all conical angles exhibits relatively integrated but faint noteworthy color bands of red, orange-yellow, and green, accompanied by the strongest broadening in the east and west directions. As the energy adjusts to high power, 60.1–70 mW, as shown in Figs. 5(e) and 5(f), we can clearly observe that the rainbow characteristics of the CSHG emission emerging from the crystal are highlighted

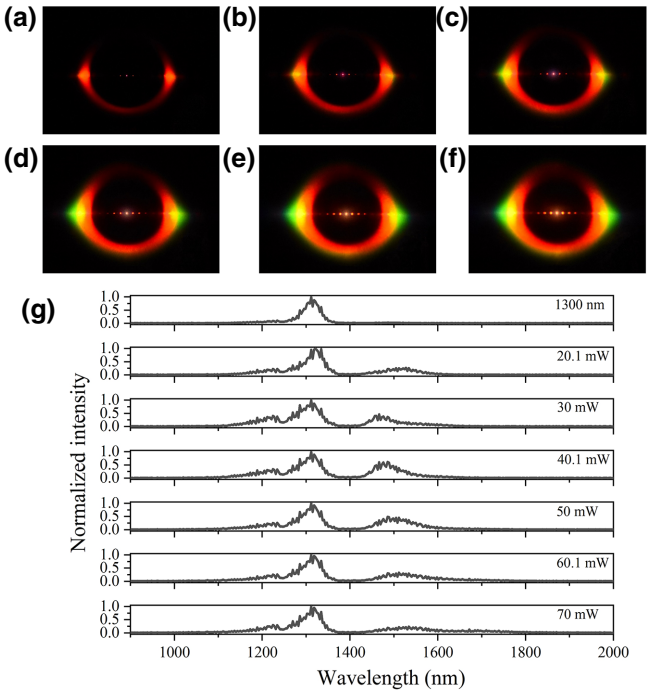

FIG. 5. Dependence of the rainbow feature of UBR CSHG emitted from the PPLN sample on the pump-laser power. (a)–(f) Projection of Cherenkov radiation driven by the near-infrared femtosecond laser at 1300 nm with different input powers, varying from 20.1 to 70 mW, with an interval of about 10 mW. (a) 20.1 mW. (b) 30 mW. (c) 40.1 mW. (d) 50 mW. (e) 60.1 mW. (f) 70 mW. (g) Original spectra at 1300 nm and spectral broadening for the pump-laser pulse with different pump powers passing through a PPLN sample.

with a superior performance of bright and well-distributed multiple bands.

The observed interesting relationship between the rainbow variation of CSHG signals and the pump-laser power can be attributed to the fact that increased pump-light power leads to enhanced 3NL within the nonlinear crystal, and thus, broadened pump-laser spectra and output CSHG spectra. As expressly illustrated in Fig. 5(g), we give the original spectrum at 1300 nm and the spectral broadening for the pump-laser pulse changing from 20.1 to 70 mW with an interval of about 10 mW when passing through a PPLN sample. It can be found that the spectrum for the pump-laser beam with an original bandwidth of 100 nm gradually expands with an increase of pump power. This strongly implies that more spectral frequency components are involved in the CSHG process and ultimately lead to broadband rainbow Cherenkov radiation when the pump power grows. The results are well reproduced by the broadband phase-matching condition of Eq. (2) and the diagram of Fig. 3(c), in which the 2NL and 3NL effects simultaneously have an effect on the CSHG process to produce rainbow CSHG patterns with enlarged bandwidth. At the same time, a larger pump power also means a higher conversion efficiency from FW to SHW and ultimately brighter CSHG rainbow patterns. These analyses visually demonstrate that the high-power ultrashort pump laser is considerably beneficial for the realization of beautiful ultrabroadband bright rainbow Cherenkov radiation through simultaneously enhanced 2NL and 3NL effects.

IV. CONCLUSIONS

We realize UBR CSHG in a single PPLN nonlinear crystal upon illumination of a high-peak-power near-infrared ultrashort femtosecond pump laser. This splendid multicolor effect involves three conspicuous colors: red, orange-yellow, and green bands. This greatly enhanced broadband capability of the UBR CSHG phenomenon, compared with an ordinary monochromatic pump configuration, can be attributed to the high peak power and broadbandwidth nature of an ultrashort femtosecond pump laser in combination with the enhancement of powerful 3NL and multiple RLVs of the PPLN crystal, so that the longitudinal phase-matching condition can be satisfied over a rich spectral range. In more detail, the following mechanisms play active roles. First, the broad spectral characteristics of an ultrashort pump laser will account for the initial broadband Cherenkov radiation. Second, new spectral components induced by 3NL, originating from the high peak power of the pump laser, further expand the bandwidth of the output CSHG signals. Third, more channels of Cherenkov radiation are enabled by the multiple-order RLVs inside the PPLN sample along the $\chi^{(2)}$ modulation direction through a phase-matched QPM CSHG process and create richer rainbow features of the CSHG. These three physical processes and mechanisms make a major contribution to the SHG Cherenkov radiation, leading to plentiful multicolored radiation patterns resembling rainbows in nature and covering 480–838 nm. Here, the most important innovation of this work is to present a flowery colorful UBR CSHG emitted from a single nonlinear optical material and automatically dispersed in space, and thus, provide a concise experimental system for generating multicolor-output ultrabroadband laser sources with tailored spatial patterns of optical fields. All observed phenomena in our experiment can find applications in nondestructive identification of domain structures, nonlinear microscopy, the monitoring of ultrashort pulses, and so on. Moreover, the efficient broadband laser-light sources implemented via such a versatile and simple noncollinear CSHG configuration are useful in nonlinear optics, nano- or microstructure formation, and laser fabrication.

ACKNOWLEDGMENTS

This work is funded by the National Natural Science Foundation of China (Grant No. 11974119), the Science and Technology Planning Project of Guangdong Province (Grant No. 2020B010190001), the Guangdong Innovative

and Entrepreneurial Research Team Program (Grant No. 2016ZT06C594), the National Key Research and Development Program of China (Grant No. 2018YFA0306200), and the Natural Science Foundation of Guangdong Province of China (Grant No. 2019A1515011605).

[1] P. A. Franken and J. F. Ward, Optical harmonics and nonlinear phenomena, Rev. Mod. Phys. **35**, 23 (1963).
[2] M. M. Fejer, G. A. Magel, D. H. Jundt, and R. L. Byer, Quasi-phase-matched second harmonic generation: Tuning and tolerances, IEEE J. Quantum Electron. **28**, 2631 (1992).
[3] D. Feng, N. B. Ming, J. F. Hong, Y. S. Yang, J. S. Zhu, Z. Yang, and Y. N. Wang, Enhancement of second-harmonic generation in $LiNbO_3$ crystals with periodic laminar ferroelectric domains, Appl. Phys. Lett. **37**, 607 (1980).
[4] B. Q. Ma, T. Wang, Y. Sheng, P. G. Ni, Y. Q. Wang, B. Y. Cheng, and D. Z. Zhang, Quasiphase matched harmonic generation in a two-dimensional octagonal photonic superlattice, Appl. Phys. Lett. **87**, 251103 (2005).
[5] B. Q. Chen, M. L. Ren, R. J. Liu, C. Zhang, Y. Sheng, B. Q. Ma, and Z. Y. Li, Simultaneous broadband generation of second and third harmonics from chirped nonlinear photonic crystals, Light: Sci. Appl. **3**, e189 (2014).
[6] B. Q. Chen, C. Zhang, C. Y. Hu, R. J. Liu, and Z. Y. Li, High-Efficiency Broadband High-Harmonic Generation from a Single Quasi-Phase-Matching Nonlinear Crystal, Phys. Rev. Lett. **115**, 083902 (2015).
[7] B. Q. Chen, L. H. Hong, C. Y. Hu, C. Zhang, R. J. Liu, and Z. Y. Li, Engineering quadratic nonlinear photonic crystals for frequency conversion of lasers, J. Opt. **20**, 034009 (2018).
[8] M. L. Ren, D. L. Ma, and Z. Y. Li, Experimental demonstration of super quasi-phase matching in nonlinear photonic crystal, Opt. Lett. **36**, 36967 (2011).
[9] A. Piskarskas, V. Smilgevičius, A. Stabinis, V. Jarutis, V. Pašiškevičius, S. Wang, J. Tellefsen, and F. Laurell, Noncollinear second-harmonic generation in periodically poled $KTiOPO_4$ excited by the Bessel beam, Opt. Lett. **24**, 1053 (1999).
[10] G. Giusfredi, D. Mazzotti, P. Cancio, and P. De Natale, Spatial Mode Control of Radiation Generated by Frequency Difference in Periodically Poled Crystals, Phys. Rev. Lett. **87**, 113901 (2001).
[11] A. R. Tunyagi, M. Ulex, and K. Betzler, Noncollinear Optical Frequency Doubling in Strontium Barium Niobate, Phys. Rev. Lett. **90**, 243901 (2003).
[12] A. Zembrod, H. Puell, and J. Giordmaine, Surface radiation from nonlinear optical polarization, Opt. Quantum Electron. **1**, 64 (1969).
[13] J. V. Jelley, *Cerenkov radiation and its applications* (Pergamon Press, New York, 1958).
[14] V. Vacaitis, Cerenkov-type phase matching in bulk KDP crystal, Opt. Commun. **209**, 485 (2002).
[15] X. W. Deng, H. J. Ren, H. Y. Lao, and X. F. Chen, Research on Cherenkov second-harmonic generation in periodically poled lithium niobate by femtosecond pulses, J. Opt. Soc. Am. B **27**, 1475 (2010).
[16] S. M. Saltiel, Y. Sheng, N. V. Bloch, D. N. Neshev, W. Krolikowski, A. Arie, K. Koynov, and Y. S. Kivshar, Cerenkov-type second-harmonic generation in two-dimensional nonlinear photonic structures, IEEE J. Quantum Elect. **45**, 1465 (2009).
[17] Y. Sheng, S. M. Saltiel, W. Krolikowski, A. Arie, K. Koynov, and Y. S. Kivshar, Cerenkov-type second-harmonic generation with fundamental beams of different polarizations, Opt. Lett. **35**, 1317 (2010).
[18] Y. Zhang, F. M. Wang, K. Geren, S. N. Zhu, and M. Xiao, Second-harmonic imaging from a modulated domain structure, Opt. Lett. **35**, 178 (2010).
[19] Y. Sheng, V. Roppo, Q. Kong, K. Kalinowski, Q. Wang, C. Cojocaru, J. Trull, and W. Krolikowski, Tailoring Čerenkov second-harmonic generation in bulk nonlinear photonic crystal, Opt. Lett. **36**, 2593 (2011).
[20] C. D. Chen, Y. Zhang, G. Zhao, X. P. Hu, P. Xu, and S. N. Zhu, Experimental realization of Cerenkov up-conversions in a 2D nonlinear photonic crystal, J. Phys. D: Appl. Phys. **45**, 405101 (2012).
[21] B. Q. Ma, B. Q. Chen, R. J. Liu, and Z. Y. Li, Multiple shape light sources generated in $LiNbO_3$ nonlinear photonic crystals with Sierpinski fractal superlattices, J. Opt. **17**, 085503 (2015).
[22] P. K. Tien, R. Ulrich, and R. J. Martin, Optical second harmonic generation in form of coherent Cerenkov radiation from a thin-film waveguide, Appl. Phys. Lett. **17**, 447 (1970).
[23] K. Hayata, K. Yanagawa, and M. Koshiba, Enhancement of the guided-wave second-harmonic generation in the form of Cerenkov radiation, Appl. Phys. Lett. **56**, 206 (1990).
[24] H. Tamada, Coupled-mode analysis of second harmonic generation in the form of Cerenkov radiation from a planar optical waveguide, IEEE J. Quantum Electron. **27**, 502 (1991).
[25] T. Suhara, T. Morimoto, and H. Nishihara, General coupled-mode analysis of Cerenkov-radiation-type second-harmonic generation in channel and fiber waveguides, IEEE J. Quantum Electron. **29**, 525 (1993).
[26] Y. Zhang, Z. Qi, W. Wang, and S. N. Zhu, Quasi-phase-matched Cerenkov second-harmonic generation in a hexagonally poled $LiTaO_3$ waveguide, Appl. Phys. Lett. **89**, 171113 (2006).
[27] Y. Zhang, Z. D. Gao, Z. Qi, S. N. Zhu, and N. B. Ming, Nonlinear Cerenkov Radiation in Nonlinear Photonic Crystal Waveguides, Phys. Rev. Lett. **100**, 163904 (2008).
[28] Y. Zhang, X. P. Hu, G. Zhao, S. N. Zhu, and M. Xiao, Cerenkov second-harmonic arc from a hexagonally poled $LiTaO_3$ planar waveguide, J. Phys. D: Appl. Phys. **42**, 215103 (2009).
[29] N. A. Sanford and W. C. Robinson, Direct measurement of effective indices of guided modes in $LiNbO_3$ waveguides using the Cerenkov second harmonic, Opt. Lett. **12**, 445 (1987).
[30] R. Ramponi, M. Marangoni, R. Osellame, and V. Russo, Nonconventional characterization of single-mode pla-

nar proton-exchanged $LiNbO_3$ waveguides by Cherenkov second harmonic generation, Opt. Commun. **159**, 37 (1999).

[31] V. Roppo, D. Dumay, J. Trull, C. Cojocaru, S. M. Saltiel, K. Staliunas, R. Vilaseca, D. N. Neshev, W. Krolikowski, and Y. S. Kivshar, Planar second-harmonic generation with noncollinear pumps in disordered media, Opt. Express **16**, 14192 (2008).

[32] S. J. Holmgren, C. Canalias, and V. Pasiskevicius, Ultrashort single-shot pulse characterization with high spatial resolution using localized nonlinearities in ferroelectric domain walls, Opt. Lett. **32**, 1545 (2007).

[33] X. W. Deng and X. F. Chen, Domain wall characterization in ferroelectrics by using localized nonlinearities, Opt. Express **18**, 15597 (2010).

[34] Y. Sheng, A. Best, H. J. Butt, W. Krolikowski, A. Arie, and K. Koynov, Three-dimensional ferroelectric domain visualization by Čerenkov-type second harmonic generation, Opt. Express **18**, 16539 (2010).

[35] B. Q. Chen, L. H. Hong, C. Y. Hu, and Z. Y. Li, White laser realized via synergic second- and third-order nonlinearities, Research **2021**, 1539730 (2021).

[36] S. M. Saltiel, D. N. Neshev, R. Fischer, W. Krolikowski, A. Arie, and Y. S. Kivshar, Generation of Second-Harmonic Conical Waves via Nonlinear Bragg Diffraction, Phys. Rev. Lett. **100**, 103902 (2008).

[37] P. Molina, M. O. Ramírez, B. J. García, and L. E. Bausá, Directional dependence of the second harmonic response in two-dimensional nonlinear photonic crystals, Appl. Phys. Lett. **96**, 261111 (2010).